Scientific paper

Capillary Transport of Water in Cracked and Non-cracked UHPFRC Specimens

Ana Mafalda Matos[1*], Sandra Nunes[2] and José L. Barroso Aguiar[3]

Received 9 February 2019, accepted 10 May 2019 doi:10.3151/jact.17.5.244

Abstract

The primary goal of the present paper is to investigate the influence of cracking on water transport by capillary suction of UHPFRC. Prismatic specimens were firstly loaded under four-point bending up to specific crack open displacement (COD). Target COD, under loading, was varied between 200 and 400 μm, in steps of 50 μm. After unloading, a COD recovery was observed with residual COD ranging between 116-334 μm and 75-248 μm for UHPFRC-1.5% and UHPFRC-3.0% specimens, respectively. The crack pattern created was characterised (number of cracks and crack width) before capillarity testing. Sorptivity results of cracked UHPFRC-1.5% and UHPFRC-3% specimens remained in the range of 0.024 to 0.044 mg/(mm^2.min$^{0.5}$), which are about 2 to 4 times higher than the sorptivity results of non-cracked UHPFRC specimens. However, the maximum sorptivity observed on cracked UHPFRC is relatively low as compared to typical sorptivity results found in good quality conventional concrete or engineered cementitious composites (ECC).

1. Introduction

Ultra-High Performance Fibre Reinforced Cement-based Composites (UHPFRC) emerged from the development of three different families of concrete, namely, self-compacting concrete (SCC), fibre reinforced concrete (FRC) and high-performance concrete (HPC) (Torregrosa 2013). The design of UHPFRC aims at a densely compacted cementitious matrix (herein referred as UHPC) using a high content of reactive powders, a minimal amount of water, a high-range water reducer and an adequate fine aggregate gradation, in order to produce high flowability and improved mechanical and durability properties (Wang *et al.* 2015). The binder of UHPC is commonly composed of Portland cement and silica fume. Due to the very low water/binder ratio (w/b) only part of the total cement hydrates. For this reason, the content of cement + silica fume in UHPC can be partially replaced by other supplementary cementitious materials (such as fly ash, blast furnace slag, metakaolin, rice husk ash, among others), in order to reduce the cost or even improve some properties of UHPC. Depending on compositions, production process and special curing conditions, the compressive, tensile and flexural strengths of UHPFRC can reach values as high as 200 to 800 MPa, 25 to 150 MPa and 30 to 141 MPa, respectively (Yoo and Banthia 2016). Nevertheless, the number of non-proprietary UHPFRC mixtures found in the literature produced with ordinary materials (minimising the use of natural resources) and room temperature curing conditions has been increasing, in an attempt to increase the general acceptance and number of applications of UHPFRC. Due to its extremely dense microstructure, the pore size distribution of UHPC basically concentrates between 2 and 3 nm (Wang *et al.* 2015); thus it is generally agreed that UHPC exhibits very excellent durability.

Most elements in concrete structures are subjected to drying and wetting cycles and are rarely saturated under service conditions. Under dry or partially saturated conditions, the rate of ingress of water, which may carry aggressive agents, is mostly controlled by capillary absorption rather than diffusion or pressure-induced flow. Therefore, flow driven by capillary suction is a significant transport process that should be considered as a criterion for long term durability of UHPFRC. The most widely used laboratory test method to assess capillary transport is the method proposed by Hall (1977), which provides a procedure to determine the rate of water absorption (also called sorptivity). Sorptivity results of sound UHPC/UHPFRC specimens found in the literature shows it is sensitive to changes in mix composition, the degree of hydration and curing conditions. Roux *et al.* (1996) observed that after 15 days of testing, total water absorbed by reactive powder concrete (RPC) remained less than 0.2 mg/mm^2, which evidences the existence of almost no capillary porosity. However, with a special curing treatment, namely, applying pressure before and during setting of UHPFRC a considerable decrease of the sorptivity coefficient (around 50%) was achieved. High curing temperatures also accelerate the hydration process, and therefore a denser matrix can be obtained in a shorter time compared with standard

[1]Ph.D. Student, CONSTRUCT-LABEST, Faculty of Engineering, University of Porto, Portugal.
*Corresponding author, *E-mail:* ana.matos@fe.up.pt
[2]Associate Professor, CONSTRUCT-LABEST, Faculty of Engineering, University of Porto, Portugal.
[3]Associate Professor, University of Minho, School of Engineering, Guimarães, Portugal.

curing, giving rise to lower sorptivity. Teichmann and Schmidt (2004) measured sorptivities of 0.03 and 0.013 mg/(mm^2×min$^{0.5}$) for water cured and heat treated UHPCs, respectively; while high-performance (C100) and normal concretes (C35) exhibited sorptivities of 0.015 and 0.08 mg/(mm^2×min$^{0.5}$), respectively. Franke *et al.* (2008) also found that UHPC exhibits a capillary water absorption 40 to 55 times lower than ordinary reference mortar (w/c=0.45). The binder composition, particularly the cement type and the incorporation of alternative SCMs in UHPC can also impact the water absorption capacity. For example, the addition of RHA (Huang *et al.* 2017) or treated bagasse ash (Rajasekar *et al.* 2018) was found to reduce the sorptivity of UHPC. Ternary blended mixtures of cement, silica fume and metakaolin might increase the water capillary absorption compared to conventional UHPFRC with cement + silica fume according to Tafraoui *et al.* (2016). However, the differences observed in these sorptivity results are not significant to cause a fundamentally different durability. Several studies reported that the addition of steel fibres decrease the sorptivity to some extent (Pyo and Kim 2017; Wang *et al.* 2018; Abbas *et al.* 2015). This is partly due to fibres bridging across the micro-flaws formed due to early ages shrinkage and the induced less connected pores (Abbas *et al.* 2015).

This superior mechanical and durability performance of UHPFRC makes it particularly suitable for use in new constructions and thin layers/jackets for strengthening and waterproofing of existing reinforced concrete structures, particularly when exposed to aggressive environments, where the durability requirements can be even more demanding than the mechanical ones (Azmee and Shafiq 2018). Indeed, a promising field of application is the rehabilitation and strengthening of reinforced concrete structures, in which a new layer of UHPFRC replaces the deteriorated concrete (cracked, carbonated, chloride attacked). The combination of existing concrete with the UHPFRC as a protective layer, which can be reinforced, provides an efficient way of increasing the durability (prolonging the service life), the stiffness and structural resistance capacity while keeping compact cross sections. Besides contributing to structural capacity, the tensile performance of UHPFRC is essential for coping with the autogenous deformations and for ensuring water-tightness even when subjected to critical tensile deformations. While a matrix cracking stress of 7 - 9 MPa ensures that the UHPFRC layers remain uncracked under restrained autogenous deformations, the hardening branch up to the (post-cracking) tensile strength of 8 - 16 MPa and strains of 0.2% - 0.4% is crucial for ensuring the low permeability even when the UHPFRC is subjected to significant mechanical actions (Charron *et al.* 2007, 2008). This tensile response mostly depends on the fibre-to-matrix bond mechanics (Wille and Naaman 2012, 2013) and the fibre distribution/orientation (Abrishambaf *et al.* 2017). If the former can be tailored during mix design, the latter is influenced by the rheology, casting method, geometry and dimensions of the specimen. Therefore, the "in-structure" tensile response can differ from that characterised in laboratory tests and cracking might occur in the UHPFRC layer. Further research is needed to study the influence of cracking on UHPFRC durability.

Only a few studies on the water transport properties of UHPFRC under applied loads (cracked state) were found in the literature. Charron *et al.* (2008) studied the permeability and the capillary absorption of UHPFRC submitted to high tensile deformations. Direct tensile tests were performed on UHPFRC prisms of 50×200×500 mm notched at mid-length. Upon reaching a predefined level of deformation, during the tensile test, the specimen was unloaded, and a core of 100 mm in diameter was extracted for absorption tests. Absorption measurements on undamaged UHPFRC specimens showed a very low value of sorptivity [0.0027 mg/(mm^2×min$^{0.5}$)], which is related to the limited amount of capillary pores in UHPFRC. Also, relatively low values were measured for specimens with a residual strain of 0.05% and 0.13% presenting sorptivity values of 0.0034 and 0.0050 mg/(mm^2×min$^{0.5}$), respectively. However, for the highest level of deformation (total displacement of 0.33 mm, in the softening domain), water capillary absorption presented an abrupt increase, with a sorptivity of 0.01 mg/(mm^2×min$^{0.5}$). In that case, the localised macro-crack within the specimens acts as a large artificial capillary pore, which increases the absorption capacity of the material considerably.

Ma *et al.* (2016) used dumbbell-shaped UHPFRC specimens in which uniaxial tensile stress of 0%, 30%, 50% and 80% percentages of ultimate tensile stress were applied. Then, specimens were unloaded, and the capillary absorption test was carried out. The sorptivity values obtained at 0%, 30%, 50% and 80% of ultimate tensile stress were 0.0012, 0.0019, 0.0026 and 0.01 mg/(mm^2×min$^{0.5}$), respectively. The number of microcracks and new pores increase with the increase of applied tensile loading, and they provide passageways for water penetration into UHPC. The increase of the maximum amount of absorbed water is not very significant when the applied tensile stress is below 50% of ultimate tensile stress; however, it becomes noticeable when the applied tensile stress reaches 80% of ultimate tensile stress (Ma *et al.* 2016).

Recently, Wang *et al.* (2018) investigated the influence of splitting tensile loading damage effect on transport properties of UHPFRC incorporating different contents of steel fibres (0%, 1%, 2% and 3%). Cylindrical specimens with 100 mm diameter and 50 mm height were subjected to different splitting loads with stress levels varying from 50% to 80% of the ultimate splitting tensile strength. Then, in the unloaded state, sorptivity and penetrable porosity were measured, and the crack pattern was characterised. As expected, sorptivity increased with a higher level of splitting load and crack

Table 1 Chemical composition and specific surface area of ECat.

Material	Chemical composition (% by mass)									Specific surface area (m^2/kg)
	SiO_2	Al_2O_3	Fe_2O_3	CaO	MgO	SO_3	Na_2O	K_2O	LOI	
ECat	40.30	54.45	0.45	0.06	0.15	0.00	0.43	0.02	1.05	150 070 (BET)

open displacement after unloading (COD_{res}). The measured sorptivity values for variable steel fibre contents are similar when the COD_{res} is lower than 20 μm, but differences were found for higher COD_{res} values (up to 100 μm). For example, the sorptivity value was 0.023, 0.018 and 0.016 mg/(mm^2.$min^{0.5}$) for the UHPC samples containing 1%, 2% and 3% steel fibres, respectively, when the COD_{res} is around 40 μm. A higher steel fibre content was found to play a positive effect on improving the transport properties of UHPFRC with the same COD_{res} value (Wang *et al.* 2018).

As mentioned above, cracking in thin UHPFRC layers might occur under service conditions, which can have a negative impact on its durability. This concern is addressed in the current paper by evaluating the water absorption by capillarity in both non-cracked and cracked UHPFRC specimens, with two different fibre contents (1.5% and 3%). After different damage levels were introduced on prismatic specimens, by means of four-point bending test (target COD ranging between 200 and 400 μm, in steps of 50 μm), the crack pattern observed on the tensile face of the specimen was characterized; and then the sorptivity tests were carried out to develop an understanding of how micro- and macro-crack formation in UHPFRC degrade its resistance to water penetration.

2. Materials and Methods

2.1 Raw materials and mixture proportions

The cement used in this study is ordinary Portland cement, Type I with a strength grade of 42.5 R, in accordance with EN 197-1. Silica fume (SF) was used with a specific surface area of 19632 m^2/kg, which has a SiO_2 content >90%, complying with the requirements of EN 13263-1. Limestone filler (98% $CaCO_3$) was also used as a fine mineral admixture, having a specific surface of 550 m^2/kg, and complying with the requirements of EN 12620. The aggregate fraction is composed of 85% siliceous natural sand (d_{max} = 1 mm) and 15% ECat (a spent equilibrium catalyst, generated by Sines Refinery, Portugal), by volume. **Table 1** presents the main chemical properties and specific surface area of ECat. ECat presents high specific surface (150 070 m^2/Kg) with water affinity giving rise to high water absorption, namely 30%, by mass. Thus, extra water for ECat's absorption was added to the mixture. More details concerning the origin of ECat can be found elsewhere (Nunes and Costa 2017). The used polycarboxylate-based superplasticizer (Sp) has a solid content of 40% and a density of 1080 Kg/m^3. High strength short steel fibres with 0.2 mm in diameter and 13 mm in length (l_f /d_f = 65) were used as reinforcement. The tensile strength and modulus of elasticity of the fibres are 2750 MPa and 200 GPa, respectively.

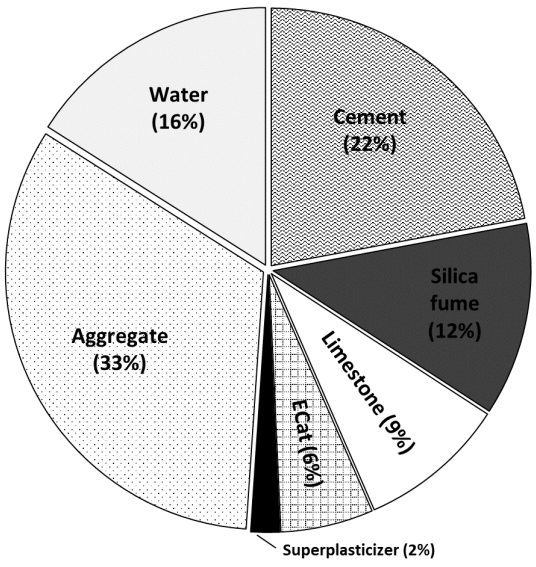

Fig. 1 Mixture proportions of non-proprietary UHPC used, in terms of volume.

Figure 1 illustrates the volume fraction of each constituent material of the non-proprietary UHPC mixture used in the current study. This UHPC mixture was optimised by the authors in a previous study, aiming at low autogenous shrinkage and high resistivity without impairing self-compatibility and compressive strength. A report of this study is under preparation for publication elsewhere. Steel fibres were added to UHPC in volume fractions of 1.5% and 3% to manufacture two UHPFRC mixtures, by replacing an equivalent volume of aggregates.

2.2 Mixing procedure, fresh state characterisation and specimens preparation

UHPFRC mixtures were produced using a mixer in accordance with EN 196-1. The mixing procedure had the following steps: (1) mixing ECat (dry state) with 80% mixing water plus ECat's water absorption (30% by mass) for 5 minutes; (2) adding sand and remaining powder materials and mixing for 2.5 minutes; (3) stopping to scrape material adhering to the mixing bowl and mixing for another 2.5 minutes; (4) introducing the rest of the water plus 75% of Sp and mixing for 2.5 minutes; (5) adding the rest of Sp and mixing for 1.5 minutes; (6) fibers incorporation and mix for 2 minutes.

Immediately after mixing, the mixtures self-compactability was assessed using the mini-slump flow test according to EFNARC recommendations (EFNARC 2005). Several prismatic specimens (40×40×160 mm) were moulded in one lift without any

Table 2 Number of prismatic specimens (40×40×160 mm) prepared for each test condition.

UHPFRC series	Flexural behaviour	Crack pattern characterisation and water capillary absorption					
		Non-cracked	Target COD_{load}				
		0 μm	200 μm	250 μm	300 μm	350 μm	400 μm
1.5%	5	3	3	3	3	3	3
3.0%	5	3	3	3	3	3	3

mechanical vibration due to the self-compacting ability of the mixtures (see the experimental plan in **Table 2**). In addition, 3 cubic specimens (50 mm) were moulded for each UHPFRC mixture to evaluate the compressive strength at 7 and 28 days. The specimens were then covered with a plastic sheet and demoulded after 1 day and then water cured in a controlled environment chamber at 20 ± 2ºC and HR ≥ 95%, until the testing age. No special curing treatment was applied to UHPFRC specimens.

2.3 Mechanical testing

The compressive strength of both UHPFRC mixtures was assessed at 7 and 28 days, following ASTM C109/C109M procedure. Three specimens were tested for each age.

Flexural strength of specimens of UHPFRCs was assessed at 28 days, through a four-point bending test. The device for applying loads (see **Fig. 2**) consists of 1) two supporting rollers; 2) two upper rollers (loading), which divide the load applied by the machine equally between the two rollers. Rollers were manufactured from steel and have a circular cross-section with a diameter of 10 mm. They are at least 10 mm longer than the width of the test specimen. The distance, I, between the outer rollers (i.e. the span) is equal to $3d$, where $d = 40$ mm is the width of the specimen. The distance between the loading rollers is equal to d. The loading rollers are equally spaced between the support rollers as shown in **Fig. 2**. All dimensions were adjusted from the test set-up suggested in EN 12390-5. The flexural strength (f_{cf}) can be computed from the maximum load sustained (F) as follows:

Fig. 2 Four-point bending test configuration and positioning of the LVDT on the lateral surface of the prism.

$$f_{cf} = \frac{F \times I}{d_1 \times d_2^2} \quad (1)$$

where $I = 120$ mm is the distance between the supporting rollers (mm), $d_1 = 40$ mm is the width of the test beam (mm) and $d_2 = 40$ mm corresponds to depth of tested beam (mm).

2.4 Cracking procedure

UHPFRC specimens cracking was produced through the four-point bending test, using the test configuration described in the previous section. Two LVDTs, with a range of 5 mm and a precision of 1.6 μm, were installed at the front and back surfaces of each specimen, perpendicular to the loading direction, to monitor the COD evolution, see **Fig. 2**. At 28 days, prismatic specimens were cracked by imposing different cracks open displacements (COD) between 200 and 400 μm, in steps of 50 μm, to obtain different crack patterns (see **Table 2**). The number of specimens used for each test condition is indicated in **Table 2**. When the target COD was achieved (COD_{load}), the specimen was unloaded and the residual COD was recorded (COD_{res}). The tests were carried out in a 300 kN Instron testing machine, under displacement control with a displacement rate of 0.003 mm/s, which was kept constant during the experiment.

After removing the specimen from the test set-up, its central part was dry cut and a smaller prism was obtained with dimensions of 40×40×(46 - 52) mm as shown in **Fig. 3**, which was then used for crack pattern characterisation and later in the water absorption by capillarity test. The specimens were referenced taking into account the fibre content, the target COD_{load} and the specimen replicate number. For example, "1.5%-200-1", corresponds to specimen number one, incorporating 1.5% steel fibres with a target COD_{load} of 200 μm.

2.5 Characterisation of the crack pattern

Before cracking the specimens, a coloured grid was marked on the tensile face of the specimen (in between the two loading points) as shown in **Fig. 3**, in order to facilitate the crack pattern characterisation. Since UHPFRC develops multiple micro-cracking before reaching the peak load, often crack path branching occurs which makes it very difficult to distinguish every single crack and to count the total number of cracks. Therefore, in this study only the cracks found over three horizontal lines [A, B and C shown in **Fig. 4(a)**] were characterised, within the central 40 mm length zone, corresponding to maximum bending moment zone. Be-

sides, the 40 mm length was subdivided into four equal segments of 10 mm length each [**Fig. 4(a)**] to allow easier localisation of each crack. This allowed organising the data of crack pattern characterisation in the form of a matrix (3×4), corresponding to 3 lines (A, B and C) by 4 columns (segments 1, 2, 3 and 4). The cracks found over each line were observed, in the unloaded state, and photographed using a Multizoom Nikon AZ100 microscope together with a PC and a DS-U2 digital camera. A Nikon-AZ Plan Fluor 5× objective was used, and the magnification range was adjusted to crack dimension. A typical photo obtained is presented in **Fig. 4(b)**. Later, using image analysis software (ImageJ), the crack width was evaluated taking six measurements along each crack, as shown in **Fig. 4(b)**. The median of the six measurements taken along each crack [see **Fig. 4(b)**] was considered in this study as the representative value of the crack width.

2.6 Capillary water absorption test

After characterising the crack pattern, the specimens were allowed to dry in a ventilated heater at 40 ± 1°C until constant mass. Specimens were weighed periodically and equilibrium was assumed when the mass loss was less than 0.05% in two consecutive measurements. Samples dried at 40°C were cooled at ambient temperature (21 ± 2°C), during 24 h before initiating the test. The mass before and after cooling was recorded and the difference was always < 0.05%, meaning constant moisture content. The time required for the conditioning regime to complete was about 7 days.

Water absorption was determined using conventional gravimetric measurement in a simple vertical capillary rise setup by monitoring the increase in sample mass over time at ambient temperature (21 ± 2°C) and following the recommendation RILEM TC 116-PCD. The testing surface of each specimen was placed on plastic rods in a tray containing shallow water to a depth of about 2-3 mm from the bottom of the prism. The measured cumulative water absorbed was plotted against the square root of elapsed time. For one-dimensional absorption into an unsaturated semi-infinite homogeneous medium, cumulative absorption is given by the following expression (Hall 1977):

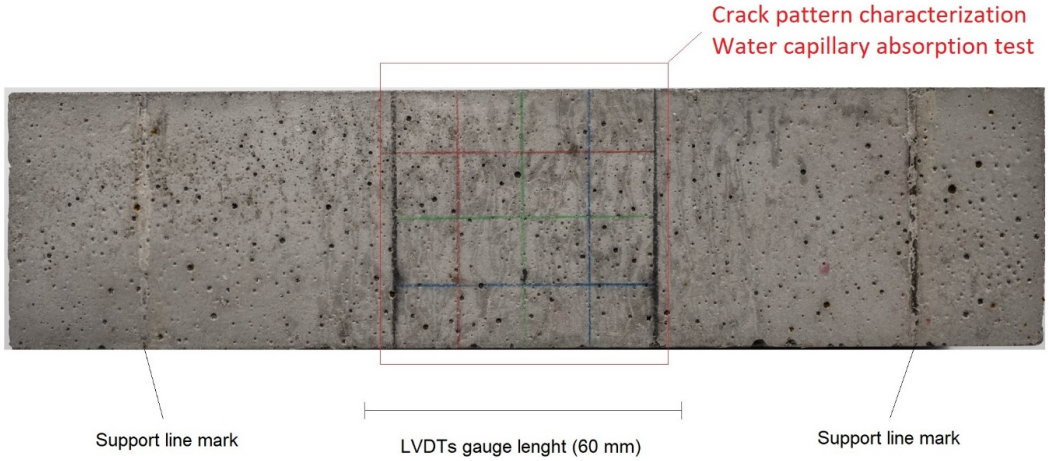

Fig. 3 Segment of the prismatic specimen used for crack pattern characterisation and sorptivity testing.

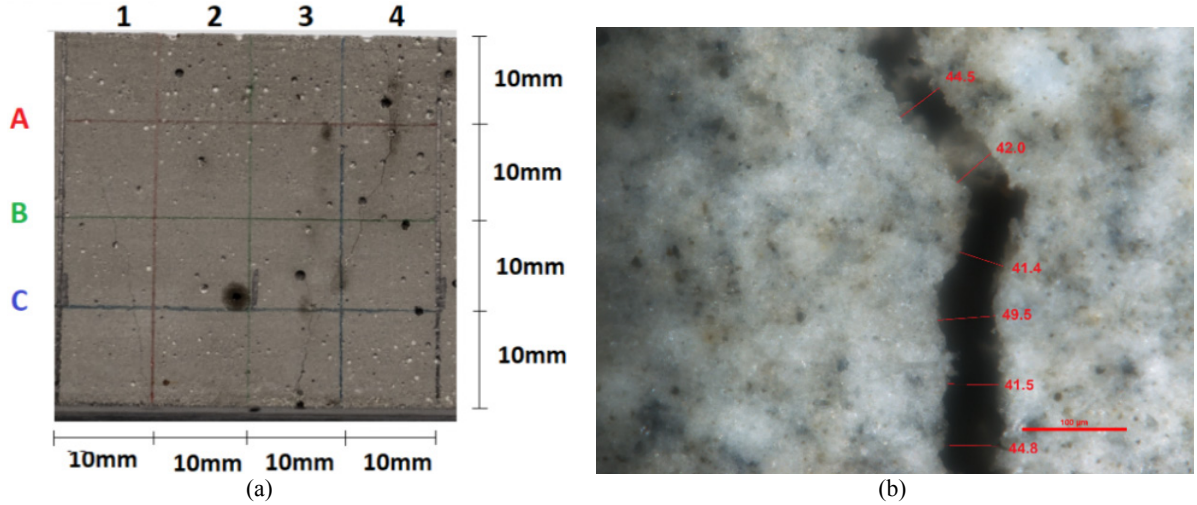

(a) (b)

Fig. 4 (a) Grid used for measuring the number of cracks and crack widths; (b) Example of a crack observed in 1.5%-350-3 specimen, and corresponding 6 measurements of the crack width.

Table 3 Slump flow diameter and compressive strength of tested mixtures.

	UHPFRC-1.5% (χ =0.9)	*UHPFRC-3.0%* (χ =1.8)
D_{flow}	302 mm	283 mm
fcm		
7 days	104 ± 5.1 MPa	118 ± 2.6 MPa
28 days	121 ± 2.5 MPa	147 ± 2.3 MPa

$\chi = \frac{Vf \times Lf}{df}$, where Vf is the volume of fibres per m^3, Lf and df are the length and diameter of fibres, respectively.

$$i = S_0 + S \times t^{0.5} \quad (2)$$

where S is the sorptivity of the material (mg/(mm^2.min$^{0.5}$)), t is the elapsed time (minutes) and S_0 (mg/mm^2) is the fitting constant. The sorptivity coefficient (S) was determined from the slope of the best-fitting line, using linear regression analysis, drawn across at least nine readings taken from the start of the test up to 4 hours. This was repeated for three replicate specimens, for each test condition. Non-cracked prisms were also tested for control purposes, for both fibre contents.

3. Results and Discussion

3.1 Workability and mechanical properties of UHPFRCs series

Concerning UHPFRC mixtures workability, spread flow diameters of 302 and 283 mm were obtained for 1.5% and 3.0% fibre contents, respectively. It is well established that the spread flow diameter decreases with an increase of the fibre factor (χ), which takes into account the combined effect of fibres aspect ratio and fibre content (Markovic 2006). For small values of the fibre factor (χ < 1.0), an increase of χ has little impact on the final spread diameter; while with higher fibre factors (χ > 2) the risk of fibre agglomeration during the mixing process increases and, consequently, an abrupt reduction of workability occurs (Marchão *et al.* 2012). By doubling the fibre content, no sudden loss of workability was observed, as could be anticipated from χ values lower than 2 (see **Table 3**).

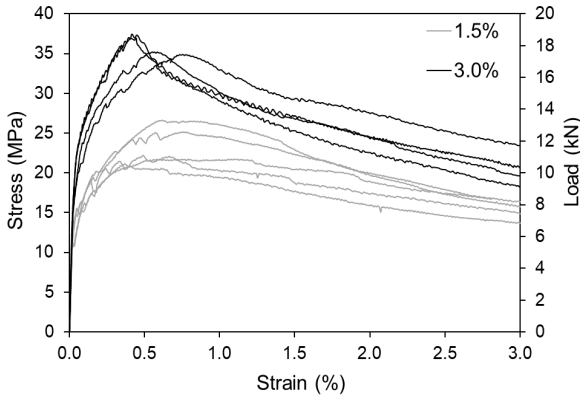

Fig. 5 Four point bending stress/load – strain relationships for all valid specimens.

Table 4 Main four-point bending test parameters for each individual specimen.

Series	Specimen	f_{cr} (MPa)	f_{cf} (MPa)	COD_{fcf} (μm)
1.5%	1	11.2	21.7	464.62
	2	11.3	20.8	244.06
	3	10.6	22.2	292.34
	4	10.2	26.6	372.02
	5	10.7	25.1	455.95
3.0%	1	15.0	34.9	454.25
	2	14.7	35.2	331.11
	3	15.0	37.5	249.41
	4	13.9	37.0	265.17

As expected, very high compressive strengths were obtained, higher than 100 MPa at 7 days and reaching 121 MPa and 147 MPa for fibre contents of 1.5% and 3.0%, respectively, at 28 days. A slight improvement of compressive strength was achieved by incorporation of higher fibre dosage. This was also found by other authors, and is attributed to the improvement of the fibre ability to delay the micro-crack formation and to arrest crack propagation (Yoo *et al.* 2013; Yoo and Banthia 2016).

Figure 5 shows the flexural behaviour of UHPFRC specimens, including the individual stress/load - strain curves for all the valid specimens. For each series, 1.5% and 3.0%, five specimens were tested, and at least four results were considered valid (the crack localised within the measuring length covered by the LVDTs). As can be observed in **Fig. 5** both mixtures exhibited flexure-hardening behaviour. The peak stresses (f_{cf}) achieved with 1.5% and 3.0% fibre contents were 23.3 ± 2.5 and 36.2 ± 1.6 MPa, respectively. The first crack (f_{cr}) occurred at stresses of 10.8 ± 0.9 and 14.7 ± 1.0 MPa for 1.5% and 3.0% fibre contents, respectively. In general, the peak stress (f_{cf}) is approximately twice the first-cracking stress (f_{cr}) (see **Table 4**). The first-cracking and the peak flexural stresses increased with the fibre content. However, the maximum load showed larger difference according to the fibre content, which is in agreement with other authors' findings (Yoo *et al.* 2013; Yunsheng *et al.* 2008; Kang *et al.* 2010; Yoo and Banthia 2016). Also, the specimens exhibiting higher peak stresses provided a more brittle behaviour in the

softening region (lower post-peak ductility), as also found by (Yoo *et al.* 2013).

The strain-hardening stage (before the peak load) is characterised by a multiple cracking formation, without localisation of any major crack. **Figure 6** illustrates the multiple cracking stage, characterised by tiny crack openings that naked eyes cannot observe, and the surface needs to be sprayed with alcohol to reveal them. After the peak load, a softening behaviour is observed, which is characterised by a macro-crack formation, as exemplified in **Fig. 7**.

3.2 Crack pattern characterisation

(1) COD recovery after unloading (COD_{load} and COD_{res})

Figure 8 and **Tables B.1** and **B.2** show the target values of COD_{load} were achieved with a reasonable approximation (± 15%), for all tested specimens. Measured values of COD_{res} as a function of COD_{load} are represented in **Fig. 9**, showing a good linear relation between COD_{res} and COD_{load} for each fibre content. A similar trend was already observed by Ma *et al.* (2016). Furthermore, lower COD_{res} values were found with the increase of fibre content, for equivalent COD_{load}.

(2) Crack pattern characterisation

The matrixes with data on measured crack widths (in μm) are presented in **Table A.1** of Appendix A, for all tested specimens. Also, a colour scale was adopted to allow easy visualisation of crack open dimension. A summary of crack pattern parameters [average number of cracks counted over lines A, B and C (*N*); minimum (Min), maximum (Max) and median crack width (Med)] is presented in Appendix B, in **Tables B.1** and **B.2** for UHPFRC-1.5% and UHPFRC-3.0%, respectively.

Concerning the number of cracks, no clear tendency was found for UHPFRC-3% specimens, but it seems they slightly increase with the damage level. The aver-

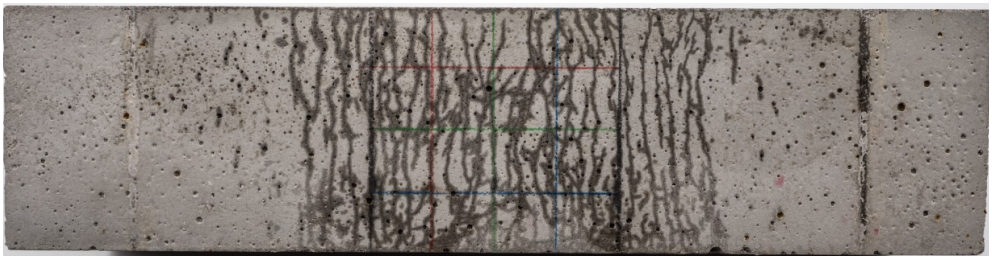

Fig. 6 Multiple cracking observed in specimen 3.0%-250-3, after spraying the surface with alcohol.

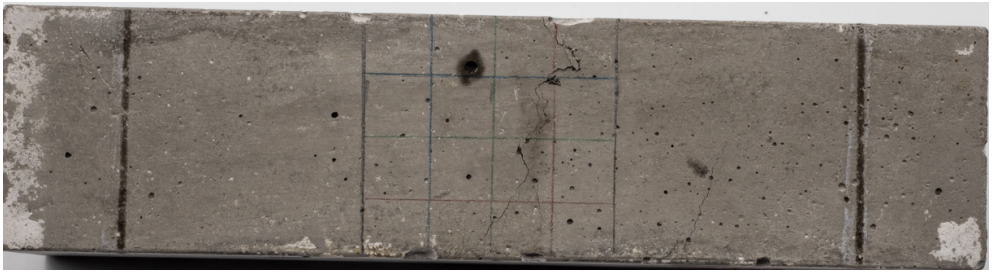

Fig. 7 Localized macro-crack (specimen 3.0%-400-2).

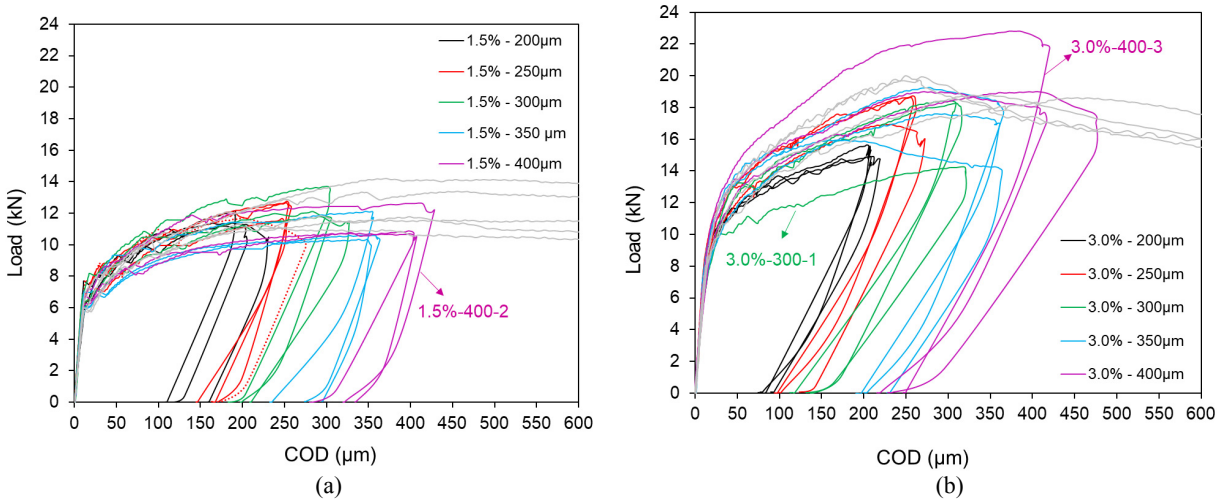

(a) (b)

Fig. 8 Load-displacement curves obtained while establishing target COD_{load}: (a) UHPFRC-1.5%; (b) UHPFRC-3%.

age number of cracks is roughly constant for UHPFRC-1.5% specimens, except for 1.5%-400-3 specimen. The average number of cracks observed over a length of 40 mm remained below 6 and 8 for UHPFRC-1.5% and UHPFRC-3% specimens, respectively, (see **Fig. 10**), except for specimen 1.5%-400-3. The median of crack width results is under 53 µm and 34 µm for UHPFRC-1.5% and UHPFRC-3% specimens, respectively, [see **Fig. 11(a)**]. This confirms that an increase of fibre content is effective to suppress the development of cracks, resulting in smaller micro-cracks. **Figure 11(b)** shows the maximum crack width results. Up to a COD_{res} of about 125 µm maximum crack width remained below 100 µm. A more significant increase of maximum crack width (> 200 µm) was observed with COD_{res} > 275 µm and COD_{res} > 200 µm for UHPFRC-1.5% and UHPFRC-3.0%, respectively.

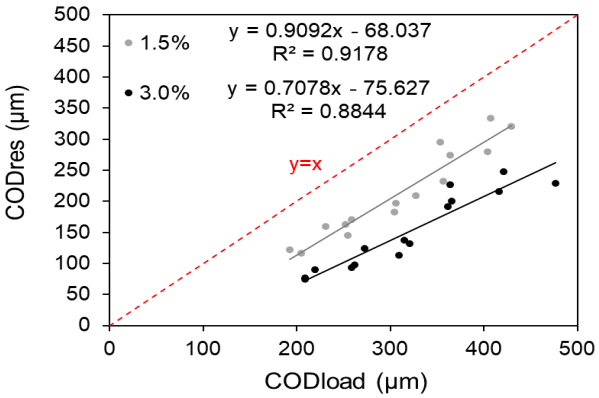

Fig. 9 Relation between COD_{load} and COD_{res}.

3.3 Water capillary absorption

Figures 12 and **13** show cumulative water absorbed (mass per unit of inflow area) against square-root of elapsed time (t) for UHPFRC with 1.5% and 3.0% fibre contents, respectively. Note that the plots show data from the first 4 hours of measurement. Besides cracked specimens, cumulative water absorbed by reference specimens (non-cracked, 0 µm) is included in the graphs. More detailed information on these test results is provided in Appendix B.

Typical pictures from specimens after 4 h water exposure are presented in **Figs. 14** and **15** for 1.5% and 3.0% specimens, respectively. In these figures a regular boundary between the wet and dry zones can be ob-

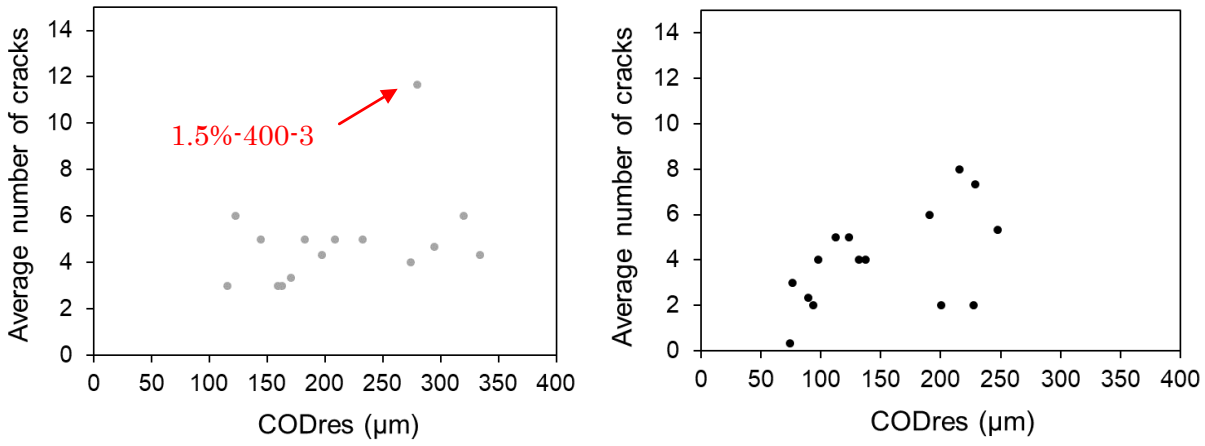

Fig. 10 Average number of cracks over the length of 40 mm for: a) 1.5% and b) 3.0%.

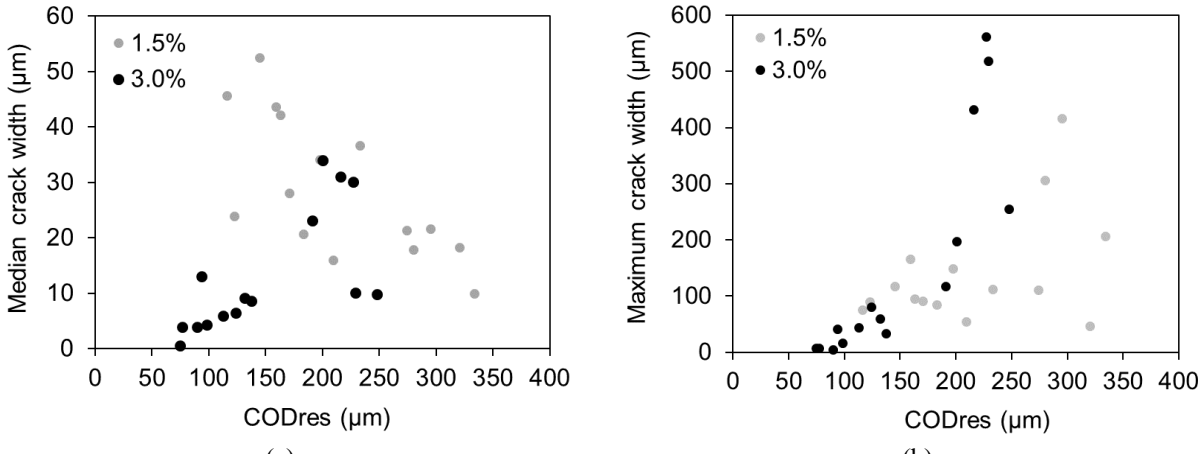

Fig. 11 (a) Median crack width; (b) Maximum crack width results.

served in control specimens (non-cracked), whereas cracked specimens presented an irregular demarcation boundary. With micro-cracks formation a wet front is observed, since the micro-cracks get fulfilled with water due to their suction capacity. When a macro-crack localizes in one of the previously formed micro-cracks, the remaining of the specimen unloads and cracks in those zones can close, thus resulting in lower suction effect. **Figures 14** and **15** show that in addition to crack width, crack length and tortuosity may also influence the sorptivity values of UHPFRC.

Figures 12 and **13** clearly show that undamaged UHPFRC specimens have a constant and very low rate of water absorption, compared to cracked specimens. The sorptivity of undamaged UHPFRC specimens was 0.0178 and 0.0076 mg/(mm^2.min$^{0.5}$) for 1.5% and 3% fibre content, respectively. These results are in agreement with results from previous research works also depicted in **Fig. 17** (Roux *et al.* 1996; Teichmann and Schmidt 2004, Huang *et al.* 2017; Rajasekar *et al.* 2018; Tafraoui *et al.* 2016; Pyo and Kim 2017; Chen *et al.* 2018). When compared to good quality conventional

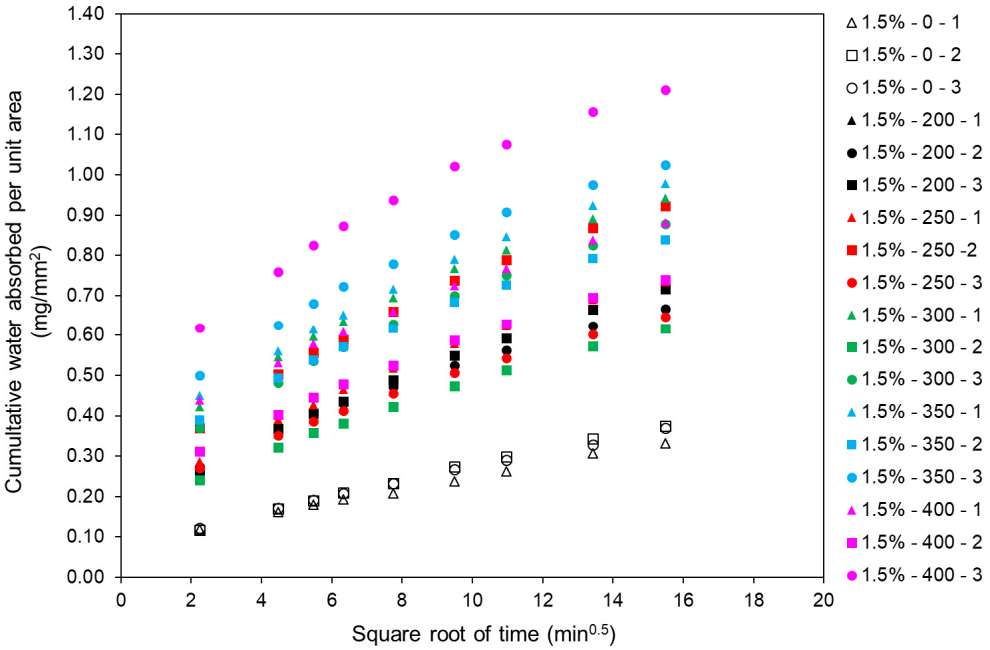

Fig. 12 Cumulative capillary water absorption of UHPFRC-1.5% specimens.

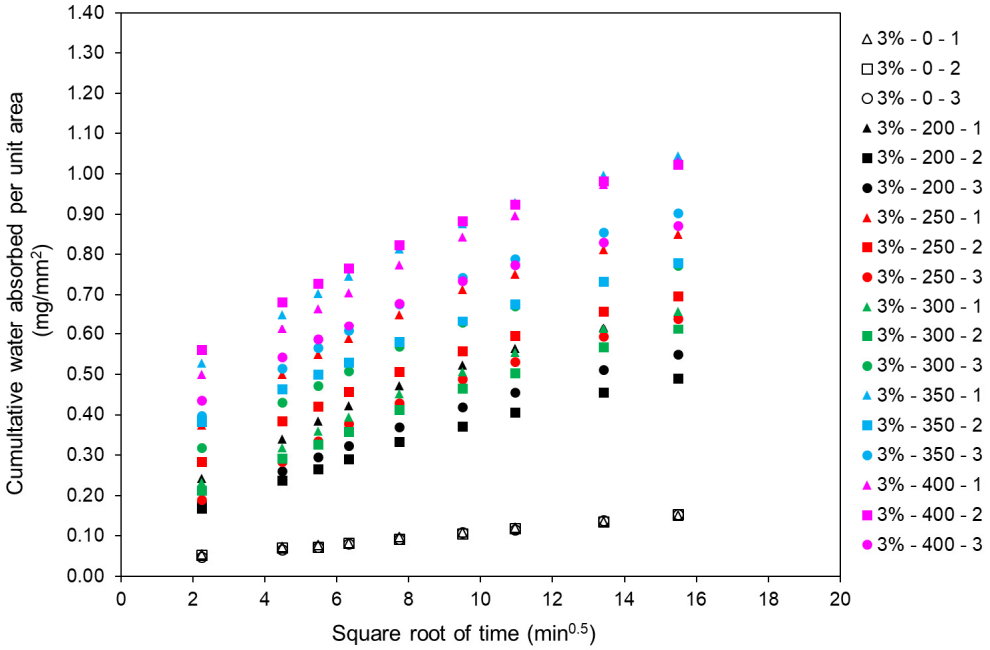

Fig. 13 Cumulative capillary water absorption of UHPFRC-3% specimens.

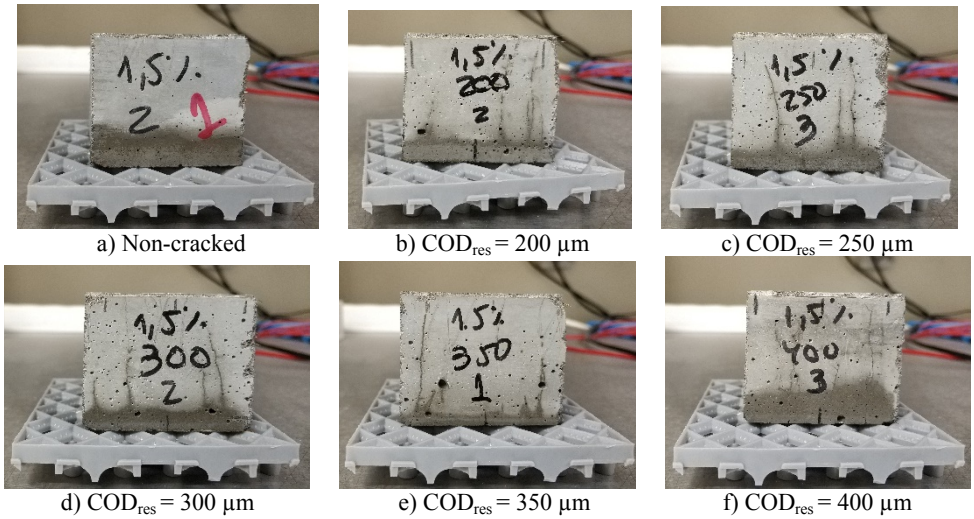

a) Non-cracked b) COD_{res} = 200 µm c) COD_{res} = 250 µm

d) COD_{res} = 300 µm e) COD_{res} = 350 µm f) COD_{res} = 400 µm

Fig. 14 Depth of water penetration after 4 h of test duration, corresponding to UHPFRC-1.5% specimens.

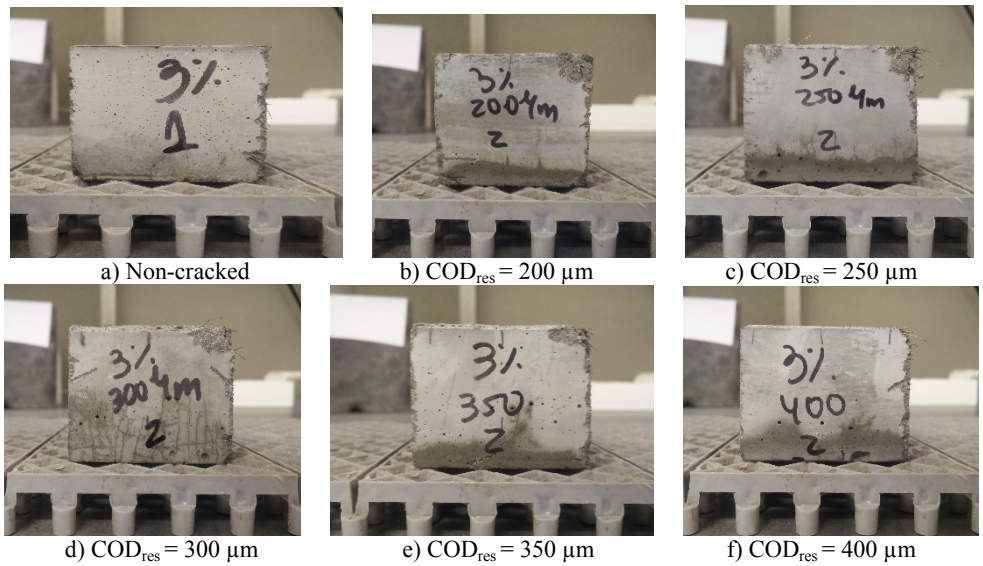

a) Non-cracked b) COD_{res} = 200 µm c) COD_{res} = 250 µm

d) COD_{res} = 300 µm e) COD_{res} = 350 µm f) COD_{res} = 400 µm

Fig. 15 Depth of water penetration after 4 h of test duration, corresponding to UHPFRC - 3.0% specimens.

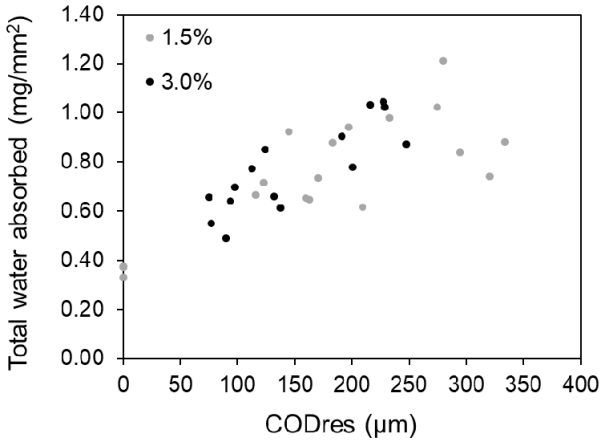

Fig. 16 Total of water absorbed during test.

concrete (w/c = 0.40), exhibiting sorptivity above 0.09 mg/(mm^2.min$^{0.5}$) (Neville 2011), or even with engineered cementitious composite (ECC) with indicative values of sorptivity around 0.028 mg/(mm^2.min$^{0.5}$) (Liu *et al.* 2016), the UHPFRCs under study presented very low sorptivities in the undamaged state (see **Fig. 17**). This may be attributed to the very low water content, the absence of coarse aggregates and the dense cementitious matrix that provide a significantly lower capillary porosity and thus capillary sorption capacity of UHPFRC.

Concerning the cracked specimens, cumulative water absorbed during the 4 h test duration and the sorptivity results are represented in **Figs. 16** and **17**, respectively, as a function of COD_{res}. In general, the total water absorbed increased with the imposed deformation, as shown in **Fig. 16**. The sorptivity results of cracked specimens exhibited less variation (15% and 13%, for 1.5% and 3% fibre contents, respectively) compared to the cumulative water absorbed results (20% and 23% for 1.5% and 3% fibre contents, respectively). From **Figs. 12** and **13**, it can be observed a significant slope change on cumulative water absorption curves compar-

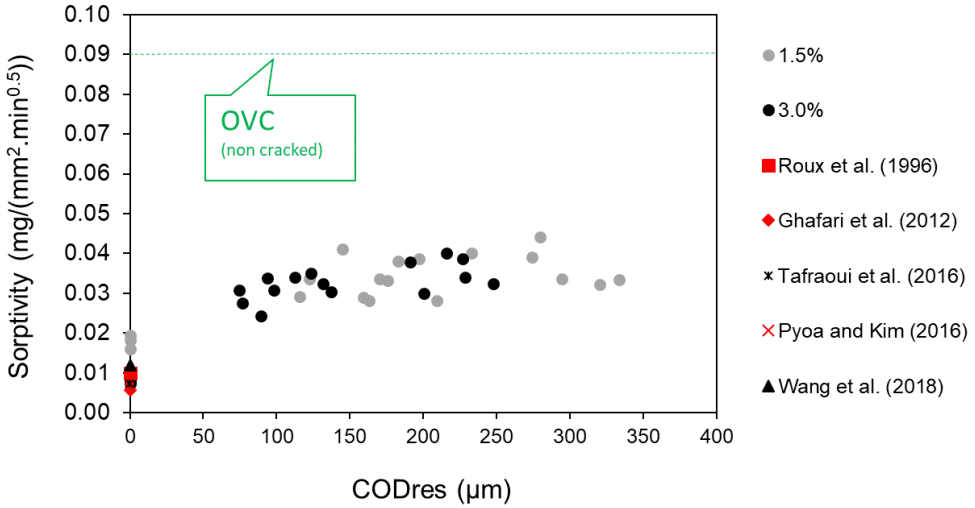

Fig. 17 Sorptivity of UHPFRCs specimens and ordinary vibrated concrete (OVC).

ing non-cracked with cracked specimens. Results of total water absorbed on cracked specimens, for a given target COD_{load}, exhibited a much larger scatter when compared to non-cracked specimens (see **Tables B.1** and **B.2**), which can be explained by the variable crack patterns and the relatively small size of the specimens. The use of larger specimens, with a potential higher number of cracks, might improve the accuracy of results. Nevertheless, it would make the crack analysis process even more time consuming. Despite some differences in terms of crack patterns, sorptivity results of cracked UHPFRC-1.5% and UHPFRC-3% specimens remained in the range of 0.024 to 0.044 (mg/(mm^2.min$^{0.5}$), respectively. In addition, the maximum measured sorptivity for the cracked UHPFRC specimens [0.044 mg/(mm^2.min$^{0.5}$)] remains relatively low when compared to that of ordinary vibrated concrete (OVC) with w/c = 0.40, as depicted in **Fig. 17**.

Finally, the sorptivity values of cracked UHPFRC specimens presented in this work possibly represent an upper limit of sorptivity in actual structures, since the effect of self-healing was not considered, due to the short experiment duration (4 h). These features provide UHPFRC with distinct barrier qualities, proving that even when cracked it can act as a protective layer increasing the durability (and service life) in the rehabilitation of structures or elements.

4. Conclusions

From the test results and analysis of cracked UHPFRC specimens, the following conclusions were established:

(1) Workability and mechanical properties:

a. UHPFRC mixtures prepared combining a non-proprietary UHPC with 1.5% and 3% steel fibres exhibited self-compacting ability, in the fresh state.
b. UHPFRC-1.5% and UHPFRC-3% mixtures exhibited a compressive strength of 147 and 156 MPa after 28 days of wet curing, respectively.
c. The four-point bending flexural strength of UHPFRC almost doubled by changing the fibre content from 1.5% to 3.0%; an average flexural strength of 36.2 and 23.3 MPa was reached, respectively. This increment of fibre content had less impact on the first cracking stress.
d. Specimens exhibiting higher peak stresses provided more brittle behaviour in the softening region (lower post-peak ductility).

(2) COD recovery and crack pattern:

a. After unloading a COD recovery was observed. Residual COD ranged between 116 - 334 µm and 75 - 248 µm for UHPFRC-1.5% and UHPFRC-3.0% specimens, respectively.
b. A good linear relation was found between COD_{res} and COD_{load} for each fibre content, the COD_{res} values being lower when the fibre content increased to 3%, for equivalent COD_{load}.
c. The average number of cracks observed over a length of 40 mm remained below 6 and 8 for UHPFRC-1.5% and UHPFRC-3% specimens, respectively.
d. The median of crack width results remained under 53 µm and 34 µm for UHPFRC-1.5% and UHPFRC-3% specimens, respectively.
e. A significant increase on maximum crack width (> 200 µm) was observed with COD_{res} > 275 µm and COD_{res} > 200 µm for UHPFRC-1.5% and UHPFRC-3.0%, respectively.

(3) Capillary water absorption:

a. Average sorptivity results of undamaged UHPFRC specimens were 0.0178 and 0.0076 (mg/(mm^2.min$^{0.5}$)) for 1.5% and 3% fibre contents, respectively. These results are in agreement with results from previous research works.
b. Despite the observed differences in terms of crack pattern, sorptivity results of cracked UHPFRC-1.5% and UHPFRC-3% specimens remained in the range of 0.024 to 0.044 mg/(mm^2.min$^{0.5}$).
c. The maximum measured sorptivity for the cracked UHPFRC specimens [0.044 (mg/(mm^2.min$^{0.5}$)] re-

mains relatively low when compared to that of conventional concrete (w/c = 0.4).

The influence of cracking on other durability indicators, such as the resistance to chlorides ingress is also under evaluation within the current project.

Acknowledgments

This work was financially supported by: UID/ECI/04708/2019- CONSTRUCT - Instituto de I&D em Estruturas e Construções funded by national funds through the FCT/MCTES (PIDDAC); by the project POCI-01-0145-FEDER-031777 – "UHPGRADE - Next generation of ultra-high performance fibre-reinforced cement based composites for rehabilitation and strengthening of the existing infrastructure" funded by FEDER funds through COMPETE2020 - Programa Operacional Competitividade e Internacionalização (POCI) and by national funds (PIDDAC) through FCT/MCTES; and by FCT - Fundação para a Ciência e a Tecnologia through the Ph.D. scholarship PD/BD/113636/2015, attributed within the Doctoral Program in Eco-Efficient Construction and Rehabilitation (EcoCoRe). Collaboration and materials supply by Sines Refinery/Galp Energia, Secil, Omya Comital, Sika, Bekaert and EUROMODAL is gratefully acknowledged.

References

Abbas, S., Soliman, A. M. and Nehdi, M. L., (2015). "Exploring mechanical and durability properties of ultra-high performance concrete incorporating various steel fiber lengths and dosages." *Construction and Building Materials*, 75, 429-441.

Abrishambaf, A., Pimentel, M. and Nunes, S., (2017). "Influence of fibre orientation on the tensile behaviour of ultra-high performance fibre reinforced cementitious composites." *Cement and Concrete Research*, 97, 28-40.

Azmee, N. M. and Shafiq, N., (2018). "Ultra-high performance concrete: from fundamental to applications." *Case Studies in Construction Materials*, 9.

Charron, J. P., Denarie, E. and Bruhwiler, E., (2007). "Permeability of ultra high performance fiber reinforced concretes (UHPFRC) under high stresses." *Materials and Structures*, 40(3), 269-277.

Charron, J. P., Denarie, E. and Bruhwiler, E., (2008). "Transport properties of water and glycol in an ultra high performance fiber reinforced concrete (UHPFRC) under high tensile deformation." *Cement and Concrete Research*, 38(5), 689-698.

Chen, Y., Yu, R., Wang, X., Chen, J. and Shui, Z., (2018). "Evaluation and optimization of ultra-high performance concrete (UHPC) subjected to harsh ocean environment: towards an application of layered double hydroxides (LDHs)." *Construction and Building Materials*, 177, 51-62.

EFNARC, (2005). "*The European guidelines for self-compacting concrete - specification, production and use*." Surrey, UK: The European Federation of Specialist Construction Chemicals and Concrete Systems.

Franke, L., Deckelmann, G. and Schmidt, H., (2008). "Behaviour of ultra-high-performance concrete with respect to chemical attack." In: E. Fehling, M. Schmidt and S. Simone Eds. *Proc. Second International Symposium on Ultra High Performance Concrete*. Kassel, Germany, 5-7 March, 2008. Kassel: Kassel University Press, 453-460.

Hall, C., (1977). "Water movement in porous building materials - I. unsaturated flow theory and its applications." *Building and Environment*, 12(2), 117-125.

Huang, H., Gao, X., Wang, H. and Ye, H., (2017). "Influence of rice husk ash on strength and permeability of ultra-high performance concrete." *Construction and Building Materials*, 149, 621-628.

Markovic, I., (2006). "*High-performance hybrid-fibre concrete - development and utilisation*." Thesis (Ph.D.). Delft University of Technology.

Kang, S., Lee, Y., Park, Y. and Kim, J., (2010). "Tensile fracture properties of an ultra high performance fiber reinforced concrete (UHPFRC) with steel fiber." *Composite Structures*, 92(1), 61-71.

Liu, H., Zhang, Q., Gu, C., Su, H. and Li, V. C., (2016). "Influence of micro-cracking on the permeability of engineered cementitious composites." *Cement and Concrete Composites*, 72, 104-113.

Ma, Z., Zhao, T. and Yao, X., (2016). "Influence of applied loads on the permeability behavior of ultra high performance concrete with steel fibers." *Journal of Advanced Concrete Technology*, 14(12), 770-781.

Marchão, C. A., Nunes, S. B., Lúcio, V. G., Bras, A. A. and Figueiras. J. A., (2012). "Development and application of a high performance fiber reinforced self-compacting concrete in post-tensioning anchorage zones." In: J. Barros Ed. *Proc. 8th RILEM International Symposium on Fibre Reinforced Concrete: Challenges and Opportunities (BEFIB 2012)*, Gamares, Portugal, 19-21 September, 2012. Bagneux, France: RILEM Publications SARL, 457-469.

Neville, A. M., (2011). "*Properties of Concrete*." 5th ed. Harlow, England: Longman Group Limited.

Nunes, S. and Costa, C., (2017). "Numerical optimization of self-compacting mortar mixture containing spent equilibrium catalyst from oil refinery". *Journal of Cleaner Production*, 158, 109-121.

Pyo, S., and Kim, H., (2017). "Fresh and hardened properties of ultra-high performance concrete incorporating coal bottom ash and slag powder." *Construction and Building Materials*, 131, 459-466.

Rajasekar, A., Arunachalam, K., Kottaisamy, M. and Saraswathy, V., (2018). "Durability characteristics of ultra high strength concrete with treated sugarcane bagasse ash." *Construction and Building Materials*, 171, 350-356.

Roux, N., Andrade, C. and Sanjuan, M. A., (1996). "Experimental study of durability of reactive powder

concretes." *Journal of Materials in Civil Engineering*, 8(1), 1-6.

Tafraoui, A., Escadeillas, G. and Vidal, T., (2016). "Durability of the ultra high performances concrete containing metakaolin." *Construction and Building Materials*, 112, 980-987.

Teichmann, T. and Schmidt, M., (2004). "Influence of the packing density of fine particles on structure, strength and durability of UHPC." In: M. Schmidt Ed. *Proc. First International Symposium on Ultra High Performance Concrete*. Kassel, Germany, 13-15 September 2004. Kassel: Kassel University Press, 313-323.

Torregrosa, C., (2013). "*Dosage optimization and bolted connections for UHPFRC ties*." Thesis (Ph.D.). Polytechnic University of Valencia.

Wang, D., Shi, C., Wu, Z., Xiao, J., Huang, Z. and Fang, Z., (2015). "A review on ultra high performance concrete: Part II. hydration, microstructure and properties." *Construction and Building Materials*, 96, 368-377.

Wang, R., Gao, X., Li, Q. and Yang, Y., (2018). "Influence of splitting load on transport properties of ultra-high performance concrete." *Construction and Building Materials*, 171, 708-718.

Wille, K. and Naaman, A. E., (2012). "Pullout behavior of high-strength steel fibers embedded in ultra-high-performance concrete." *ACI Materials Journal*, 109(4), 479-488.

Wille, K. and Naaman, A. E., (2013). "Effect of ultra-high-performance concrete on pullout behavior of high-strength brass-coated straight steel fibers." *ACI Materials Journal*, 110(4), 451-462.

Yoo, D. and Banthia, N., (2016). "Mechanical properties of ultra-high-performance fiber-reinforced concrete: a review." *Cement and Concrete Composites*, 73, 267-280.

Yoo, D., Lee, J. and Yoon, Y., (2013). "Effect of fiber content on mechanical and fracture properties of ultra high performance fiber reinforced cementitious composites." *Composite Structures*, 106, 742-753.

Yunsheng, Z., Wei, S., Sifeng, L., Chujie, J. and Jianzhong, L., (2008). "Preparation of C200 green reactive powder concrete and its static-dynamic behaviors." *Cement and Concrete Composites*, 30(9), 831-838.

Appendix A

Table A.1 Localisation of cracks observed in UHPFRC specimens and corresponding crack widths (in µm).

Target COD_{load}		UHPFRC 1.5%				UHPFRC 3.0%			
		1	2	3	4	1	2	3	4
200 µm	1	A	73		32	7			
		B	166 55						
		C	107 75 10 32 6		24				
	2	A	22		55 52	4		2 3	5
		B	54	19	46 45				
		C	76		10		4 4 4		
	3	A	57	52	85	3 3		4	4
		B	50	24	64	17	3	5	3
		C	24 24 24 24 24 24	24	89	17		4 4	5 8
250 µm	1	A	16	105 19			81 70		4 10
		B	11	39 30			10 6	8	
		C	11	11 37 56			5 17 80 31 6	3 5 2 2	
	2	A	48	43	16		4		4
		B		7 5 5 5 39		47 50			
		C	28	91	6	46 28	2 4 8 16 8	4 3 5	6
	3	A	56 80			25 17		41 3 14	
		B	117		53			12 17	
		C	63 44		44			21 15	
300 µm	1	A		123 45 58		13		11 11	6 13 24
		B	19	50	149 98			9 11	6 5
		C	12 23			34 24 29		60 21	6
	2	A	27	2 8 9 12	12	34		4 21	5 9
		B	54	14 6		54		6 33	14
		C	17 22	16 44				9	15
	3	A	21 56 6 53		38 7 3	16			6 11 44 5
		B	22 60 10			13			19 9 5 5
		C	85 5			25	13	30 4 6	12

Target COD_{load}		UHPFRC 1.5%				UHPFRC 3.0%			
		1	2	3	4	1	2	3	4
350 µm	1	A 11 B 15 8 C 112 21 6	39 35 29	89	61 69 39 9 44 78	A B C 2	190 27 197 2	 103 34	
	2	A 190 31 B 8 9 393 C	5 134 3 417	2	62 3 13 62	A 561 B C 31 156 18 25	 	 	
	3	A 110 B 21 19 25 C	 3	30 21 44 3	 3 1	A B 3 3 C	4 5 	4 66 32 55 	79 4 56 77 3 5 14 36 117 56
400 µm	1	A 206 B 114 C	1 1 	2 10	13 7 7 15 205 192 9	A 2 3 B 3 6 C	3 3 2 3 	27 57 132 5 64 31 27 73 6 35 72 64 31 67 7	 3
	2	A 1 B 9 C 7	5 36 40 40	2 11 24 2 36 25	46 43 16 18	A B C 9 36 32 190	5 69 4 50 78 13	4 49 85 3 3 11 2 519 9	3 5 5
	3	A 8 33 B 12 15 9 100 3 C 3 5 5 49 18 44 3	62 21 18 5 	71 40 33 15 27 3	306 38 13 2 91 2 5 32 18 175 7	A B 13 C 3 5 5	255 46 29 6 16 14	22 32	2 2 7 5

Legend:

0 - 50 µm

51 - 100 µm

101 - 200 µm

> 200 µm

Appendix B

Table B.1 Summary of test results for UHPFRC-1.5% series.

Specimen	*N*	Crack width (μm)			Cracking procedure			Capillary water absorption test			
		Med.	Min.	Max.	COD_{load} (μm)	COD_{res} (μm)	Maximum Load (kN)	Total water absorbed (mg/mm^2)	S ((mg/mm^2)/min$^{0.5}$)	S_0 (mg/mm^2)	R^2
1.5% - 0 - 1								0.332	0.016	0.089	0.997
1.5% - 0 - 2								0.375	0.019	0.083	0.996
1.5% - 0 - 3								0.370	0.018	0.090	0.997
1.5% - 200 - 1	3	44	6	166	231	159	11.38	0.653	0.029	0.224	0.986
1.5% - 200 - 2	3	46	10	76	205	116	11.20	0.666	0.029	0.234	0.987
1.5% - 200 - 3	6	24	3	89	192	122	12.12	0.716	0.034	0.217	0.991
1.5% - 250 - 1	3	28	5	91	258	170	12.66	0.734	0.034	0.242	0.985
1.5% - 250 - 2	5	53	17	117	255	145	12.76	0.922	0.041	0.321	0.982
1.5% - 250 - 3	3	42	7	95	252	163	11.69	0.647	0.028	0.228	0.991
1.5% - 300 - 1	4	34	12	149	306	197	11.79	0.943	0.039	0.377	0.982
1.5% - 300 - 2	5	16	2	54	327	209	12.09	0.617	0.028	0.198	0.992
1.5% - 300 - 3	5	21	3	85	304	183	13.70	0.878	0.038	0.319	0.985
1.5% - 350 - 1	5	37	6	112	356	233	12.11	0.979	0.040	0.390	0.987
1.5% - 350 - 2	5	22	2	417	354	295	10.35	0.839	0.034	0.346	0.985
1.5% - 350 - 3	4	21	1	110	364	274	10.59	1.024	0.039	0.456	0.977
1.5% - 400 - 1	4	10	1	206	407	334	10.73	0.882	0.033	0.389	0.988
1.5% - 400 - 2	6	18	1	46	429	320	12.63	0.740	0.032	0.264	0.988
1.5% - 400 - 3	12	18	2	306	404	280	10.89	1.212	0.044	0.571	0.976

Table B.2 Summary of test results for UHPFRC - 3.0% series.

Specimen	N	Crack width (μm)			Cracking procedure			Capillary water absorption test			
		Med.	Min.	Max.	COD_{load} (μm)	COD_{res} (μm)	Maximum Load (kN)	Total water absorbed (mg/mm^2)	S ((mg/mm^2)/min$^{0.5}$)	S_0 (mg/mm^2)	R^2
3.0% - 0 - 1								0.151	0.007	0.039	0.998
3.0% - 0 - 2								0.154	0.008	0.034	0.997
3.0% - 0 - 3								0.154	0.008	0.030	0.999
3.0% - 200 - 1	1	1	0	7	208	75	15.65	0.656	0.031	0.210	0.973
3.0% - 200 - 2	2	4	2	5	219	90	14.89	0.491	0.024	0.132	0.989
3.0% - 200 - 3	3	4	2	8	209	77	14.89	0.549	0.028	0.142	0.987
3.0% - 250 - 1	5	6	2	81	273	124	16.96	0.849	0.035	0.349	0.962
3.0% - 250 - 2	4	4	2	16	262	98	18.71	0.697	0.031	0.249	0.979
3.0% - 250 - 3	2	13	2	41	259	94	18.65	0.641	0.034	0.145	0.980
3.0% - 300 - 1	4	9	3	60	321	132	14.28	0.659	0.032	0.182	0.986
3.0% - 300 - 2	4	9	3	33	315	137	18.27	0.613	0.030	0.161	0.991
3.0% - 300 - 3	5	6	4	44	310	113	18.41	0.772	0.034	0.282	0.975
3.0% - 350 - 1	2	30	18	561	364	227	15.96	1.045	0.039	0.486	0.975
3.0% - 350 - 2	2	34	2	197	366	200	19.27	0.778	0.030	0.335	0.990
3.0% - 350 - 3	6	23	3	117	362	191	17.60	0.903	0.038	0.354	0.975
3.0% - 400 - 1	8	31	2	432	416	216	19.00	1.032	0.040	0.442	0.987
3.0% - 400 - 2	7	10	2	519	477	229	18.99	1.023	0.034	0.532	0.967
3.0% - 400 - 3	5	10	2	255	421	248	22.81	0.871	0.032	0.404	0.972